Available online at www.sciencedirect.com
ScienceDirect
Trans. Nonferrous Met. Soc. China 29(2019) 1569−1582

Transactions of
Nonferrous Metals
Society of China
www.tnmsc.cn

Grain structure and tensile property of Al−Li alloy sheet caused by different cold rolling reduction

Yun-long MA[1,2], Jin-feng LI[1,3], Feng-jian SANG[1], Hong-ying LI[1], Zi-qiao ZHENG[1], Cheng HUANG[4]

1. School of Materials Science and Engineering, Central South University, Changsha 410083, China;
2. Beijing Institute of Aerospace Systems Engineering, Beijing 100076, China;
3. Key Laboratory of Nonferrous Materials Science and Engineering of Ministry of Education, Central South University, Changsha 410083, China;
4. Light Alloy Research Institute, Central South University, Changsha 410083, China

Received 15 October 2018; accepted 6 June 2019

Abstract: The effect of cold rolling reduction (50%−90%) on the grain structures of solutionized 1445 Al−Li alloy sheet at 525−575 °C was investigated through electron backscatter diffraction (EBSD). Although the solutionization temperature is elevated to 575 °C, the sheet is not completely recrystallized. The main recrystallization model is subgrain coalescence and growth, and the non-recrystallization is due to the formed nano-sized $Al_3(Sc,Zr)$ dispersoids, which pin the grain boundaries, subgrain boundaries and dislocations. With increasing the cold rolling reduction, the fraction and size of the recrystallized grains in the sheet solutionized at 525 °C are decreased, but the fraction of the subgrains is increased, leading to a decrease in the fraction of the deformed structures. Meanwhile, the number fraction of high-angle boundaries (HABs) is increased. Due to the decreased fraction of the deformed structures and increased fraction of the HABs, the T8-aged 1445 Al−Li alloy sheet displays a decrease trend in the strength and heterogeneity with increasing the cold rolling reduction. At higher solutionization temperature of 575 °C, the fraction of the recrystallized grains and their size are obviously increased.

Key words: Al−Li alloy; grain structure; recrystallization; strength; cold rolling reduction

---

1 Introduction

Al−Li alloys possess unique combination of mechanical properties including low density, high elastic modulus and rather high specific strength [1]. To improve their performance including weight reduction, fuel economy, loadlifting capacity, Al−Li alloys are considered as prospective structural materials for aircraft and aerospace engineering. Up to now, three generations of Al−Li alloys have been developed. Among them, the third generation Al−Li alloys, including 2195, 2050, 2099 and 2198, have been successfully applied in launch vehicles and aircrafts [2,3].

In order to improve the structural adaptability of the Al−Li alloys, it is critical to control their microstructures. An important method for microstructure control is the adjustment of main alloying elements of Cu and Li, which determine the type, fraction and precipitation kinetics of the strengthening precipitates [4]. To modify the precipitate distribution, micro-alloying elements of Mg, Ag and Zn are added in some Al−Li alloys. In the presence of Mg, the precursors of Mg−Cu phase form and transform into a mixture of GPB/S' (Al_2CuMg) phases, and favor the formation of a dense distribution of $T1$ (Al_2CuLi) precipitates [5]. Ag or Zn element is usually added with the combination of Mg. For example, the combination of Mg+Ag is added to 2195, 2050 and 2198 Al−Li alloys [6−8], and that of Mg+Zn is added to 2099, 2199 and 2A97 Al−Li alloys [9,10]. Small amounts of Zr and Mn are added in most Al−Li alloys, which play an important role in controlling recrystallization [11−13]. In addition, Sc is a trace element used in some Al−Li alloys developed by Russia, such as 1421, 1460, 1461 and 1469 Al−Li alloys [14]. In Al−Mg and Al−Zn−Mg alloys, Sc addition enhances strength through grain refinement, $Al_3(Sc,Zr)$ particle precipitation and substructure strengthening [15−20]. In

---

Corresponding author: Jin-feng LI; Tel: +86-13278861206; E-mail: lijinfeng@csu.edu.cn

DOI: 10.1016/S1003-6326(19)65064-8

some Al−Cu−Li alloys, it was reported that the Sc addition hampered recrystallization during homogenization and displayed positive effect on the strength because of the precipitation of nano-sized $Al_3(Sc,Zr)$ particles [21,22]. However, in some other Al−Cu−Li types of Al−Li alloys, it was not found to effectively inhibit the recrystallization. On the contrary, it displayed negative effect on the strength due to the formation of coarse W (Al_8Cu_4Sc) phases and the absence of the $Al_3(Sc,Zr)$ dispersoids [23]. MA an LI [24] proposed that the small addition of rare earth (RE) elements including Sc could display positive effect on the strength of Al−Cu−Li alloys with low Cu/Li ratio, in which the δ' (Al_3Li) phases were the main strengthening precipitates.

The small Sc addition is very effective in controlling the recrystallization of heat-treatable Al−Zn−Mg alloys during annealing and solutionization process due to the formation of $Al_3(Sc,Zr)$ particles [25]. It is significant to design Al−Li alloy sheet with un-recrystallized grain structures after solutionization through small Sc addition. Recently, a new Al−Li alloy 1445 with low Cu concentration and small Sc addition was developed in Russia [26], and its aging precipitates were investigated [27]. It is significant that this alloy is suitable for thin sheets through cold rolling. For the production of thin sheets, it is critical to know the effect of cold reduction on the final structures. This work was therefore concentrated on the grain structures of the thin sheet with different cold reductions after solutionization at different temperatures. The effect of the cold reduction on the strength of the aged sheet was also investigated.

2 Experimental

2.1 Materials and procedures

The experimental alloy ingot was prepared through melting and casting. The raw materials included pure metals of Al, Cu, Li, Mg, Ag and Ni, and intermediate alloys of Al−2%Sc, Al−10%Mn, Al−4%Zr and Al−10%Ti (mass fraction). The chemical compositions of the alloy were analyzed by inductively coupled plasma optical emission spectrometer (IOP-EOS), as given in Table 1. The alloy ingot was homogenized at 470 °C for 8 h followed by heating at 520 °C for 24 h. After homogenization, the ingot with thickness of 25 mm was rolled into plate with 5.6 mm in thickness through hot rolling. After annealing, the plate was then cold-rolled to sheets with thickness of 2.6, 1.6, 1.1 and 0.6 mm. The corresponding cold rolling reductions were about 50%, 70%, 80% and 90%, respectively.

Table 1 Chemical compositions of studied 1445 Al−Li alloy (mass fraction, %)

Cu	Li	Mg	Ag	Mn	Sc	Zr	Ni	Ti	Al
1.5	1.7	0.9	0.1	0.1	0.08	0.1	0.07	0.1	Bal.

Some sheets with different cold reductions were solutionized at 525 °C for 1 h followed by quenching in water and then subjected to a two-step T8 temper (first-step aging at 150 °C for 4 h followed by second-step aging at 170 °C for 24 h after 6% pre-deformation through cold rolling). Other sheets were solutionized for 1 h at 525, 555 and 575 °C, respectively.

2.2 Tensile tests

The tensile properties of the T8-aged samples were measured. The test samples with a parallel section gauged 30 mm in length and 8 mm in width were cut from the sheets. Yield strength, tensile strength and elongation of the samples were characterized using an MTS 858 universal testing machine with a strain rate of 1.0×10^{-3} s^{-1} at ambient temperature. Three tensile tests were done for each condition to ensure the tensile data reliability.

2.3 Structure observation

The samples for metallographic observations were cut from the solutionized sheets. The longitudinal section were mechanically grounded and polished, washed ultrasonically with ethanol, and then anodically treated at 24 V in a solution containing 1.1 g H_3BO_3, 95 mL H_2O and 3 mL HF. The metallographic observations were performed with an optical microscope (OM, Leica DMI300 M).

The grain structures were also observed by electron backscatter diffraction (EBSD) with a scanning step size of 0.7 μm. The EBSD observation was performed using a Sirion 200 field emission gun scanning electron microscope (FESEM) equipped with an integrated EBSD system, at an accelerating voltage of 25 kV. The OIM Analysis 5.31 software was utilized to analyze the received EBSD data. During the data analysis, a cleanup with grain tolerance of 2° was applied to re-indexing the data points, and two kinds of boundaries were defined. Low-angle boundary (LAB) was defined at a misorientation (θ) in the range of 2°−10° ($2°<\theta<10°$), while high-angle boundary (HAB) was defined as $\theta>10°$.

Samples for transmission electron microscopy (TEM) observation were prepared by mechanical grinding and twin-jet electropolishing in a solution containing 30% nitric acid and 70% methanol (volume fraction) at −25 °C with a voltage of 15−20 V. The observations were carried out through a Tecnai G^{2}20 TEM operating at 200 kV through selected area electron diffraction (SAED) and conventional dark-field (DF) imaging. Some TEM observations were performed on a scanning transmission electron microscopy (STEM, Titan G^{2}60-300, FEI) with spherical aberration correction, and the STEM observation was operated at 300 kV.

3 Results

3.1 Solutionized grain structures after different cold reductions

Figure 1 shows the metallographic image and EBSD images of the 1445 Al−Li alloy sheet with 50% cold reduction after solutionization at 525 °C. The grains display a fiber-like morphology with some small equi-axed grains (Fig. 1(a)), indicating incomplete recrystallization. In the inverse pole figure (IPF, Fig. 1(b)) detected through EBSD, the black lines represent HABs (θ>10°), while thin white lines LABs (θ<10°). It is clear that inside some elongated grains surrounded by HABs, there exist many concentrated LABs, which actually are dislocation arrays. According to the boundaries with different misorientations, different structures in the solutionized sheet can be distinguished. For this difference, some definitions are made as follows. The criterion for subgrain boundary is defined as θ_c=2°, and that for grain boundary is θ_{GB}=10°. Meanwhile, the average misorientation inside one grain (area) is defined as θ_0. If θ_0 is larger than θ_c (=2°) inside one grain, the grain is classified as deformed grain. In one area surrounded by LAB, if θ_0 is less than θ_c (=2°), but its misorientation with neighbour area is higher than 2°, this area is defined as substructured grain (subgrain). The other grains are defined as recrystallized grains. According to this definition, the recrystallized grains, subgrains and deformed structures are therefore distinguished, as shown in Fig. 1(c). The blue color represents recrystallized grains, and the yellow color means subgrains. In addition, the thin black lines represent LABs, which correspond to thin white lines in Fig. 1(b). The red color embed with thin black lines therefore means deformed parts. The EBSD analysis result indicates that only partial recrystallization occurs in the solutionized 1445 Al−Li alloy sheet with 50% cold reduction.

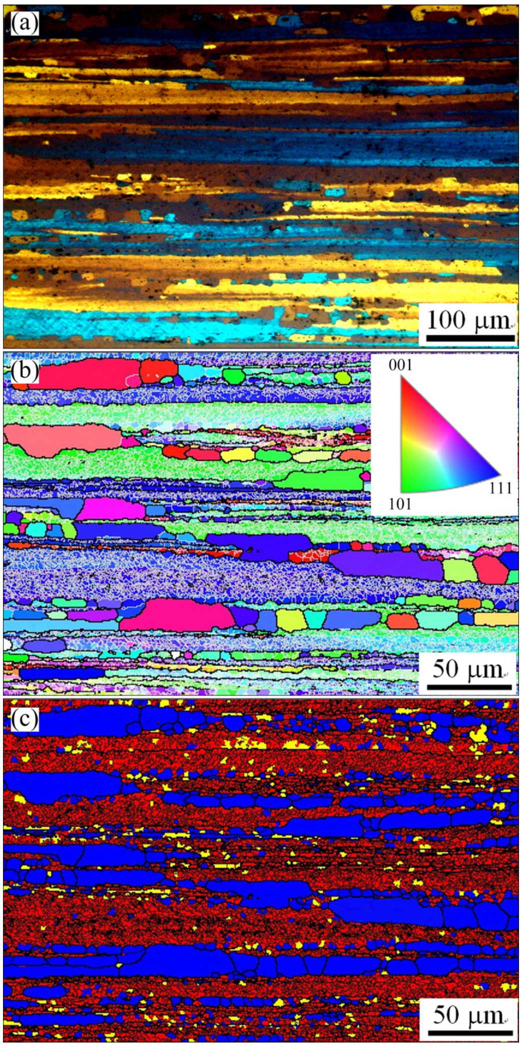

Fig. 1 Metallographic image (a) and EBSD images showing IPF (b) and structure distribution (c) of 1445 Al−Li alloy sheet with 50% cold reduction after solutionization at 525 °C

Figures 2, 3 and 4 show the metallographic images and EBSD images of the 1445 Al−Li alloy sheets with 70%, 80% and 90% cold reductions after solutionization at 525 °C, respectively. According to the metallographic images (Fig. 2(a), Fig. 3(a), Fig. 4(a)), all the samples display non-recrystallization features, i.e., fiber-like or elongated grains. The difference lies in larger grain aspect ratio of the sample with larger cold reduction.

In the EBSD images (Figs. 2(b, c), Figs. 3(b, c), Figs. 4(b, c)), the LABs are represented by thin white lines. At 70% cold reduction, it is obvious that the fraction of the recrystallization (blue color in Fig. 2(c)) and the recrystallized grain size are decreased as compared to those at 50% cold reduction. As the cold reduction is increased to 80%, it seems that the fraction of the subgrains (yellow color in Fig. 3(c)) is increased a little.

As the cold reduction is further increased to 90%, the fraction of the recrystallization (blue color in Fig. 4(c)) is obviously decreased, but that of the subgrains (yellow color) is greatly increased. In addition, the recrystallized grain size is further decreased.

The metallographic and EBSD observations indicate that incomplete recrystallization occurs in the solutionized 1445 Al−Li alloy sheets. The fraction of different structures and the recrystallized grain size are different due to different cold reductions, as shown in Fig. 5. In Fig. 5(a), the fractions of the recrystallization, sub-grains and deformed structure are remarked with

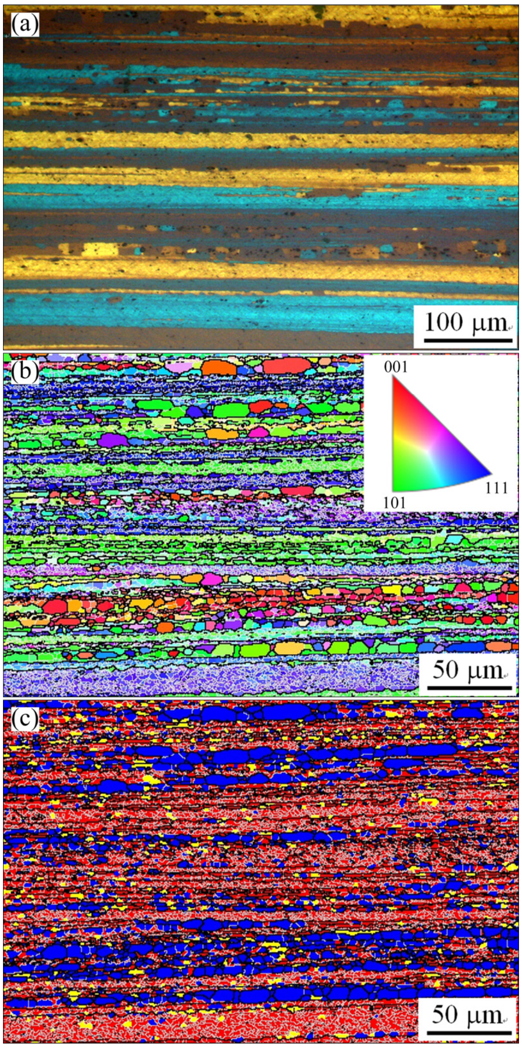

Fig. 2 Metallographic image (a) and EBSD images showing IPF (b) and structure distribution (c) of 1445 Al−Li alloy sheet with 70% cold reduction after solutionization at 525 °C

blue color, yellow color and red color, respectively. It is clear that the fraction of the recrystallization is decreased with increasing the cold reduction. However, it displays an increase tendency in the fraction of the subgrains, which is accompanied with a decrease trend in the fraction of the deformed structures. Another important feature is that the recrystallized grain size displays a decrease trend with increasing the cold reduction (Fig. 5(b)). In addition, the maximum size of the recrystallized grains shows a much greater decrease than the minimum size.

Figure 6 shows the misorientation angle distribution (MAD) histogram of the 1445 Al−Li alloy sheet with different cold reductions after solutionization at 525 °C according to the EBSD analysis. A bimodal feature with a large fraction of LABs ($2°<\theta<10°$) and a much little fraction of HABs ($50°<\theta<60°$) is observed. Meanwhile, as the cold reduction increases from 50% to 80% and 90%, the number fraction of the HABs is obviously increased.

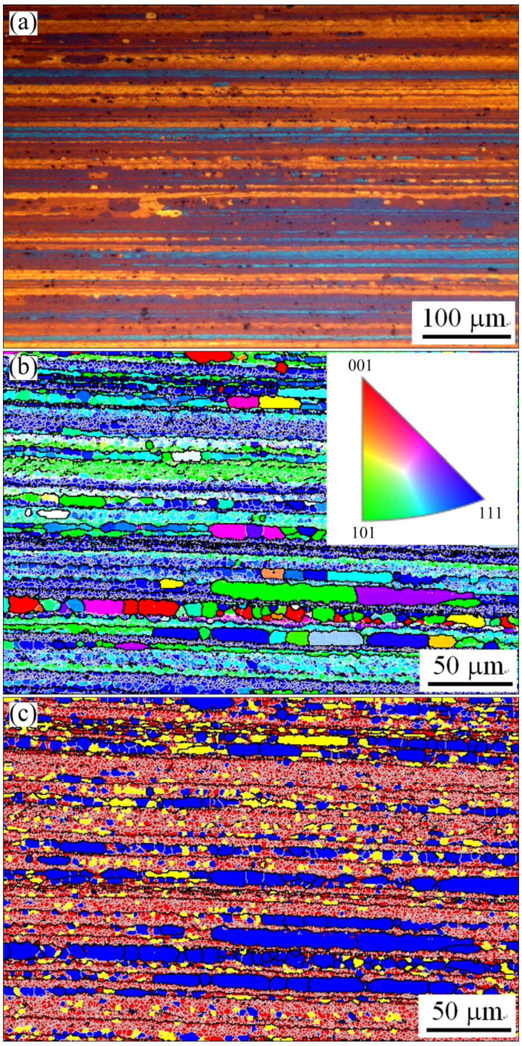

Fig. 3 Metallographic image (a) and EBSD images showing IPF (b) and structure distribution (c) of 1445 Al−Li alloy sheet with 80% cold reduction after solutionization at 525 °C

Usually, at a larger cold reduction, the recrystallization degree should be increased, due to higher stored energy caused by the cold deformation. However, in this case, it seems to be a discrepancy that at a high cold reduction of 90%, the fraction of the recrystallized grains is smaller.

3.2 Solutionized grain structures at different solutionization temperatures

Figure 7 shows the metallographic images of the 1445 Al−Li alloy sheets with 50%−90% cold reduction after solutionization for 1 h at 555 and 575 °C. When being solutionized at 555 °C, all the sheets show non-recrystallization feature, i.e., fiber-like (elongated) grains. It seems that as the cold reduction is increased from 50% to 90%, the grain size along the thickness

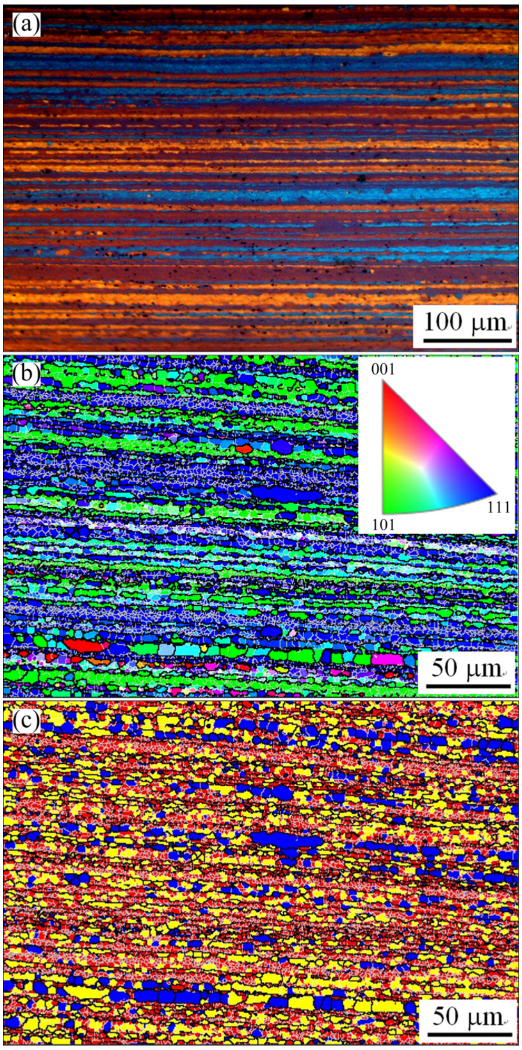

Fig. 4 Metallographic image (a) and EBSD images showing IPF (b) and structure distribution (c) of 1445 Al−Li alloy sheet with 90% cold reduction after solutionization at 525 °C

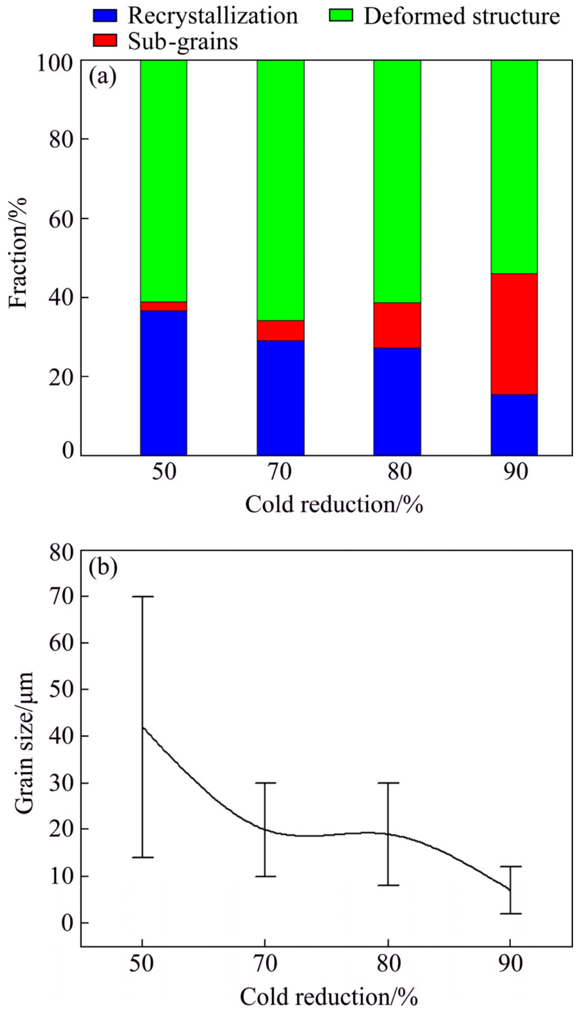

Fig. 5 Fraction of different structures (a) and recrystallized grain size (b) of 1445 Al−Li alloy sheet with different cold reductions after solutionization at 525 °C

direction is decreased, i.e., the grain aspect ratio is increased. Furthermore, no evidence indicates that the recrystallization degree is increased with the cold reduction.

As the solutionization temperature is elevated to 575 °C, although the grains still show elongated features, there exist a lot of small equiaxed grains in the solutionized sheets. That is to say, the recrystallization degree of the sheets solutionized at 575 °C is greater than that solutionized at 525 and 555 °C. Especially, in the sheet with 90% cold reduction after solutionization at 575 °C, although fiber-like grains still exist, the number of the equiaxed grains greatly increases, indicating that the recrystallization degree increases to a much high level.

Figure 8 shows the IPF maps and structure distribution of the 1445 Al−Li alloy sheets with 50% cold reduction after solutionization for 1 h at 555 and 575 °C. At both temperatures, there exist deformed structures surrounded by HABs. As the solutionized temperature is elevated from 525 (Figs. 1(b, c)) to 555 °C (Figs. 8(a, b)), it seems that there is little difference in the fraction of deformed structures (red color) and recrystallized grains (blue color). As the solutionization temperature is further elevated to 575 °C, the fraction of the recrystallized grains is significantly increased (Figs. 8(c, d)). Figure 9 shows the fraction of different structures and recrystallized grain size at different solutionization temperatures according to the EBSD analysis. The fractions of the recrystallization, sub-grains and deformed structure are remarked with blue color, yellow color and red color, respectively. As the solutionization temperature is elevated from 525 to 575 °C, the fraction of the recrystallization enlarges from 35% to 60% (Fig. 9(a)), and the average size of the recrystallized grains is increased from 37 to 50 μm

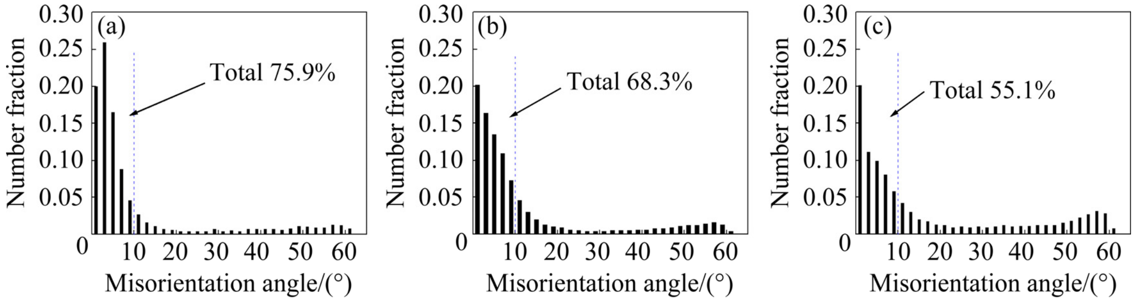

Fig. 6 Misorientation angle distribution (MAD) histogram of 1445 Al−Li alloy sheet with different cold reductions after solutionization at 525 °C: (a) 50%; (b) 80%; (c) 90%

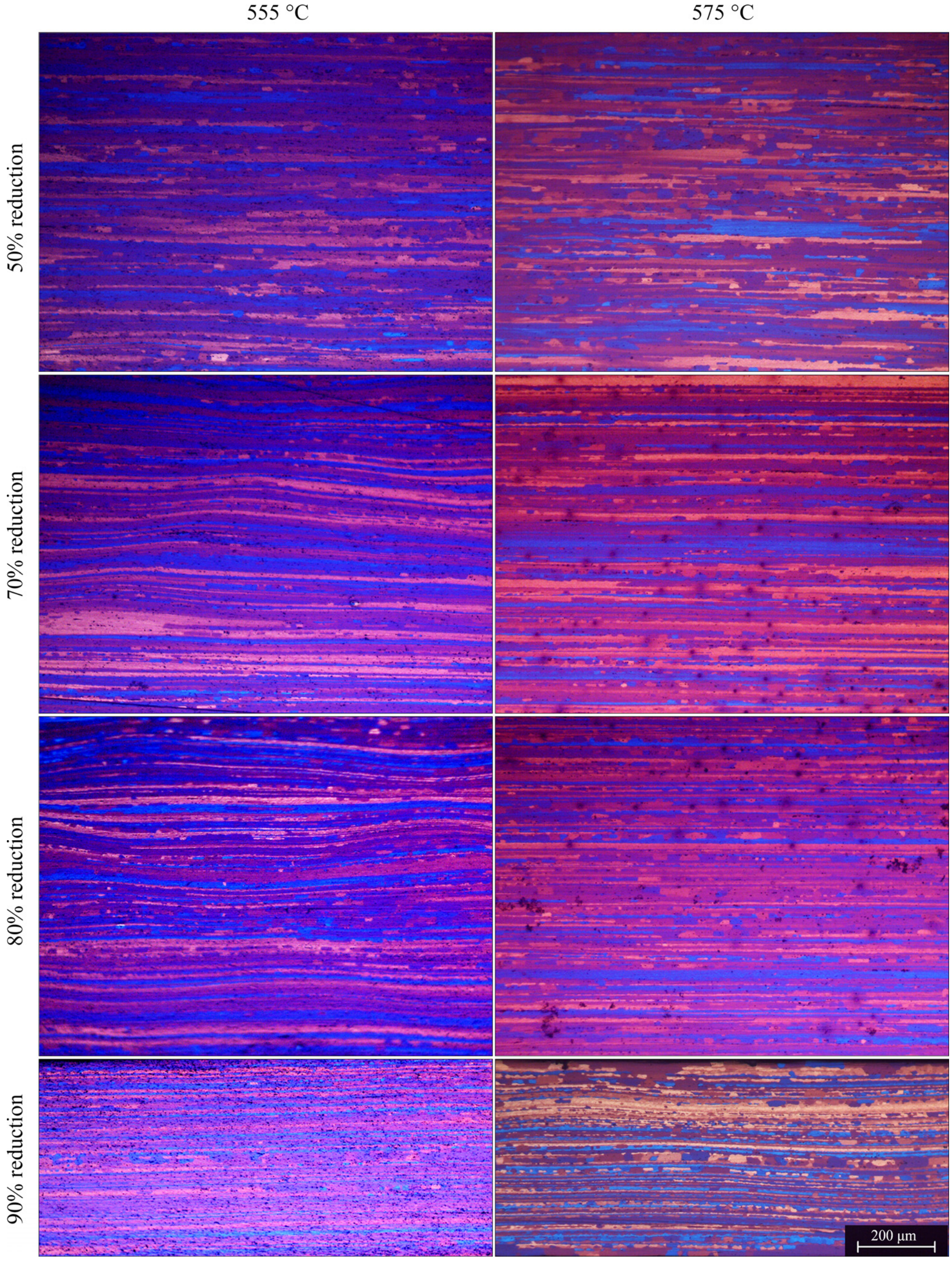

Fig. 7 Metallographic images of 1445 Al−Li alloy sheets with cold reduction of 50%−90% after solutionization for 1 h at 555 and 575 °C

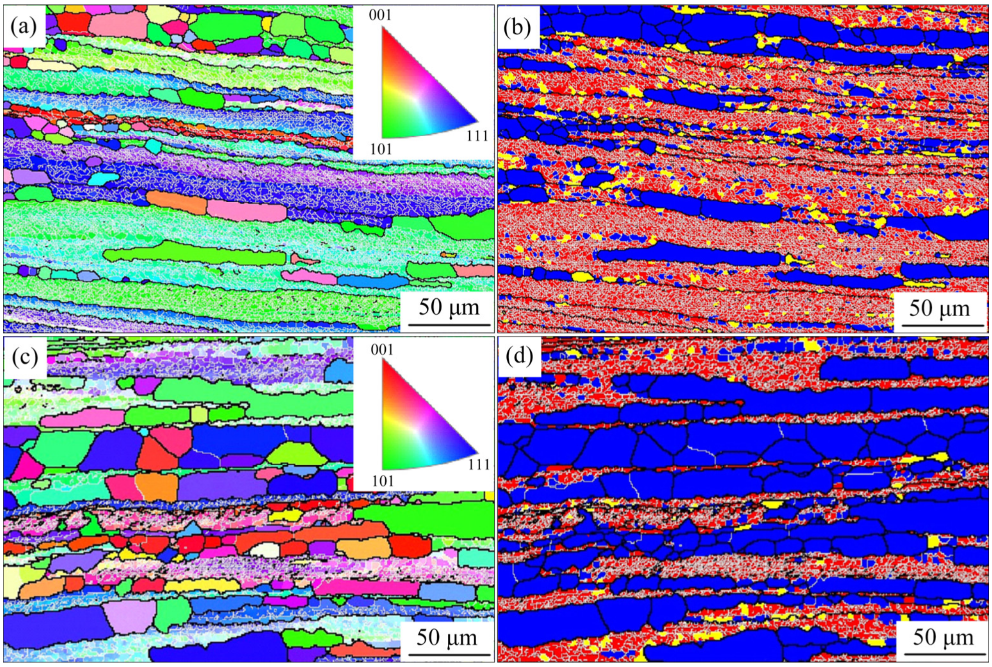

Fig. 8 EBSD images showing IPF (a, c) and structure distribution (b, d) of 1445 Al−Li alloy sheets with 50% reduction after solutionization for 1 h at 555 °C (a, b) and 575 °C (c, d)

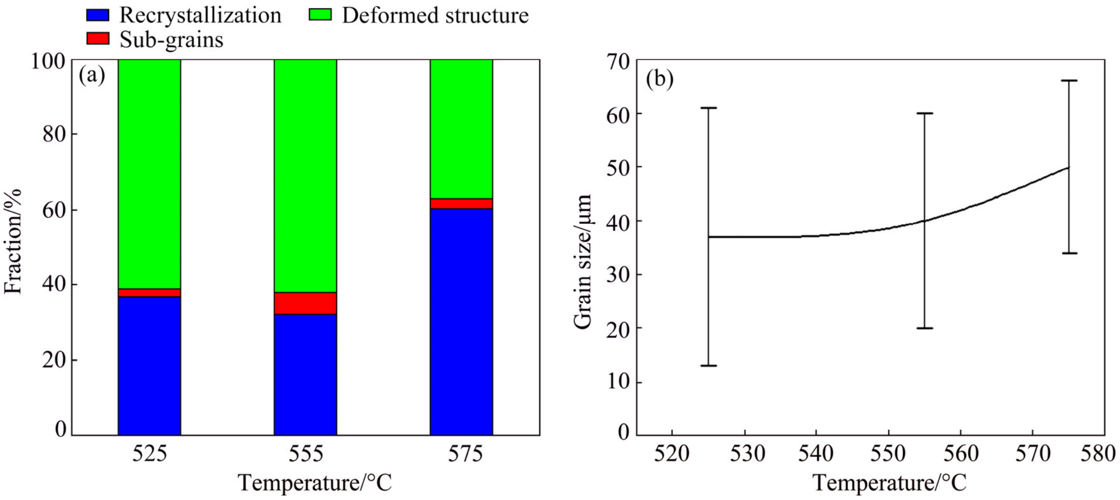

Fig. 9 Fraction of different structures (a) and recrystallized grain size (b) of 1445 Al−Li alloy sheet with 50% cold reduction after solutionization at different temperatures

(Fig. 9(b)). In addition, the minimum recrystallized grain size increases more significantly than the maximum recrystallized grain size.

Figure 10 shows the MAD histogram of the 1445 Al−Li alloy sheet with 50% cold reductions after solutionization at 555 and 575 °C according to the EBSD analysis. It is shown that the number fraction of the HABs is increased at a higher solutionization temperature of 575 °C.

3.3 Tensile property variation with cold reduction

After solutionization at 525 °C followed by a two-step T8-aging, the 1445 Al−Li alloy sheets with different cold reductions exhibit different tensile properties. Figure 11 shows the tensile curves of the T8-aged 1445 Al−Li alloy sheet with different cold reductions along longitudinal and transverse directions, which shows a significant effect of the cold reduction on the tensile properties. Table 2 shows the corresponding tensile property values. It is evident that both the tensile strength and the yield strength of the T8-aged alloy along the longitudinal direction are sequentially lowered with increasing the cold reduction. As the cold reduction increases from 50% to 90%, the average tensile strength and yield strength along the longitudinal direction are lowered from 473 and 406 MPa to 423 and 376 MPa,

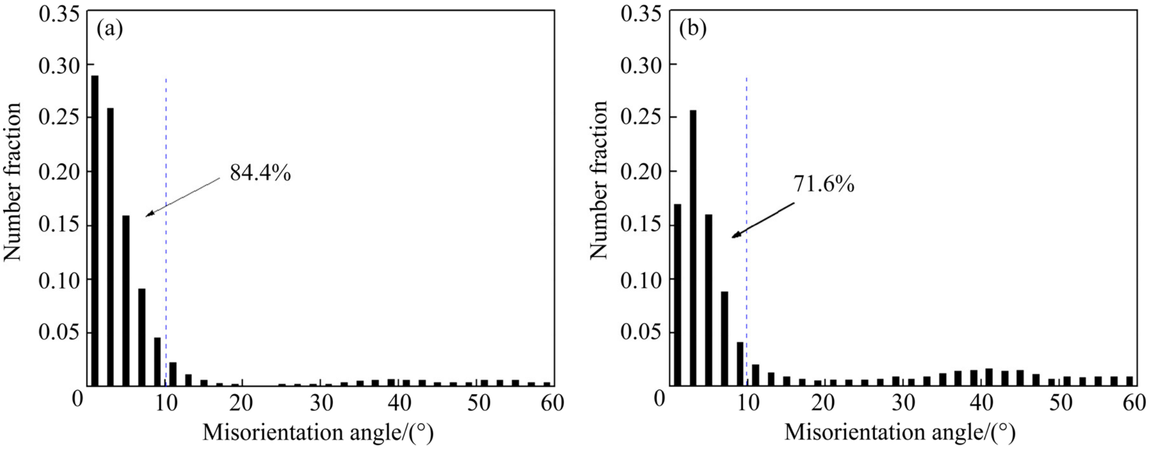

Fig. 10 MAD histogram of 1445 Al−Li alloy sheet with 50% cold reduction after solutionization at 555 °C (a) and 575 °C (b)

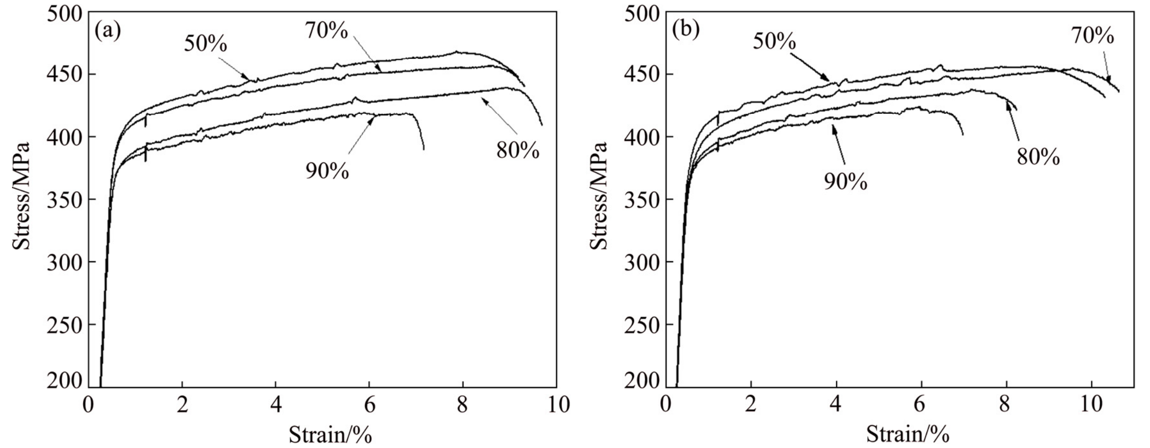

Fig. 11 Tensile curves of 1445 Al−Li alloy sheets with different cold reductions along longitudinal (a) and transverse (b) directions after two-step T8 aging following solutionization at 525 °C

Table 2 Tensile property values of 1445 Al−Li alloy sheets with different cold reductions after two-step T8 aging following solutionization at 525 °C

Cold reduction/%	Direction	Tensile strength/MPa	IPA of tensile strength/%	Yield strength/MPa	IPA of yield strength/%
50	Longitudinal	473	3.8	406	2.9
	Transverse	455		394	
70	Longitudinal	457	1.1	399	2.3
	Transverse	452		390	
80	Longitudinal	437	−0.2	380	−0.3
	Transverse	438		381	
90	Longitudinal	423	0.9	376	−0.8
	Transverse	419		379	

respectively. The strength variation along the transverse direction shows a similar trend. Because it was reported that the temperature of non-equilibrium solidus of the 1445 Al−Li alloy was 532 °C [26], the strength of the aged alloy after solutionization at 555 and 575 °C were not measured.

The heterogeneity parameter (IPA, H) is calculated according to the following equation:

$$H=(I_0-I_{90})/I_0\times100\%$$

where I_0 means the property value along the longitudinal direction; I_{90} means the property value along the transverse direction. The IPA of the T8-aged 1445 Al−Li alloy sheets with different cold reductions is also presented in Table 2, which shows a smaller heterogeneity at higher cold reduction of 80% and 90%.

4 Discussion

4.1 Recrystallization model of 1445 Al−Li alloy sheet

It is known that the recrystallization models of deformed metals include subgrain coalescence, subgrain growth and grain boundary bending [28]. Figures 12 and 13 show the magnified local IPFs and structure (recrystallized grains, subgrains and deformed structures) distribution of the 1445 Al−Li alloy sheets with 50% and 80% cold reductions after solutionization at 525 °C. In the sheet with 50% cold reduction, the main recrystallization model is subgrain coalescence and growth. It is found that some recrystallized zones are formed through subgrain coalescence and growth, which is clearly observed from the area marked with dashed ellipse (Figs. 12(a, b)). In addition, the grain boundary bending model is also observed, as indicated with the arrows in Figs. 12(c, d).

As the cold reduction is increased, according to Fig. 3, the main recrystallization model is still subgrain coalescence and growth. However, the model of grain boundary bending is also found, as shown with the arrows in Figs. 12(e, f). It is noted that the recrystallization area caused by grain boundary bending is much small.

For the 1445 Al−Li alloy sheet with 50% cold reduction, as the solutionization temperature is elevated to 555 °C, the main recrystallization model is still subgrain coalescence and growth, but the grain boundary bending model can also be distinguished, as indicated with the arrows in Figs. 13(a, b). As the solutionization temperature is further elevated to 575 °C, the model of subgrain coalescence and growth exists, but the fraction of the recrystallization caused by the grain boundary bending seems to increase (indicated with the arrows in Figs. 13(c, d)).

It is known that the driving force for the recrystallization is stored energy caused by cold plastic deformation, and the recrystallization resistance is associated with Zener pinning of secondary particles on grain boundaries, subgrain boundaries and dislocations.

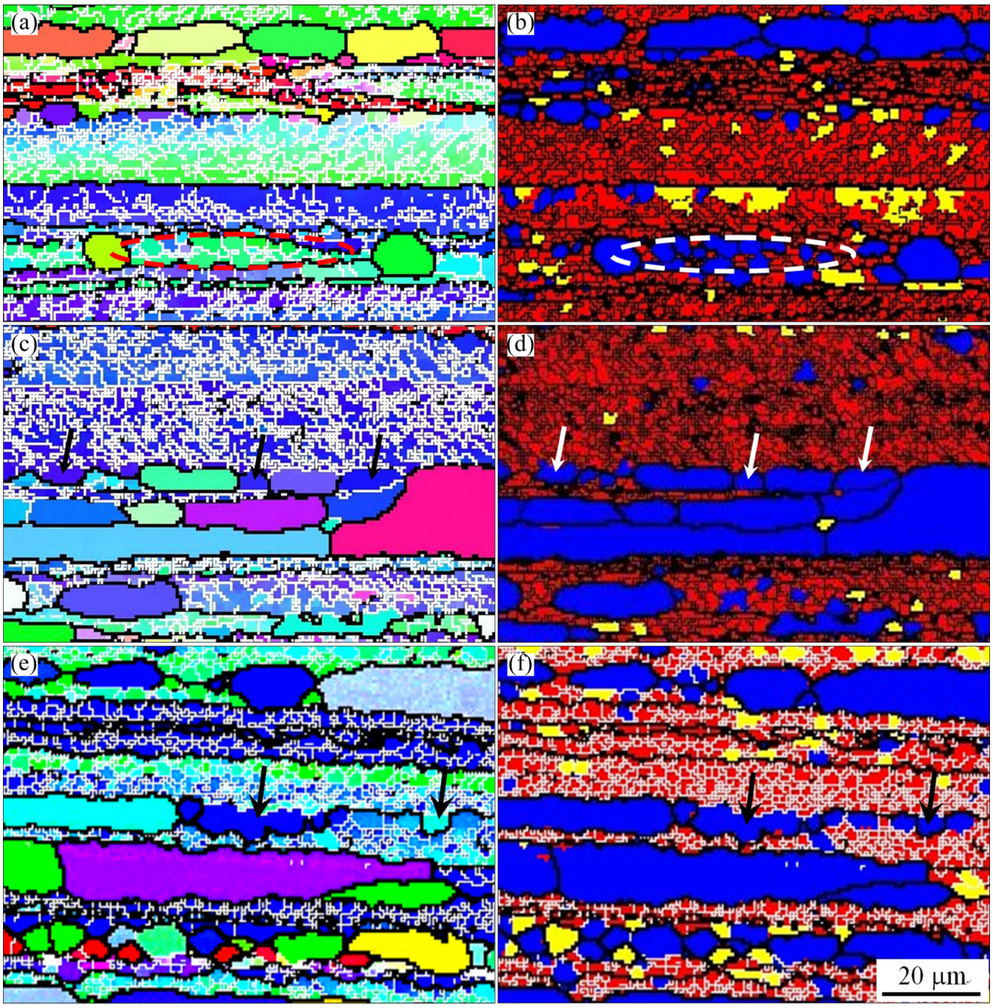

Fig. 12 Magnified local IPF (a, c, e) and structure distribution (b, d, f) of sheet with 50% (a, b, c, d) and 80% (e, f) cold reductions after solutionization at 525 °C: (a, b) Subgrain coalescence and growth model indicated with dashed ellipse; (c, d, e, f) Grain boundary bending model indicated with arrows

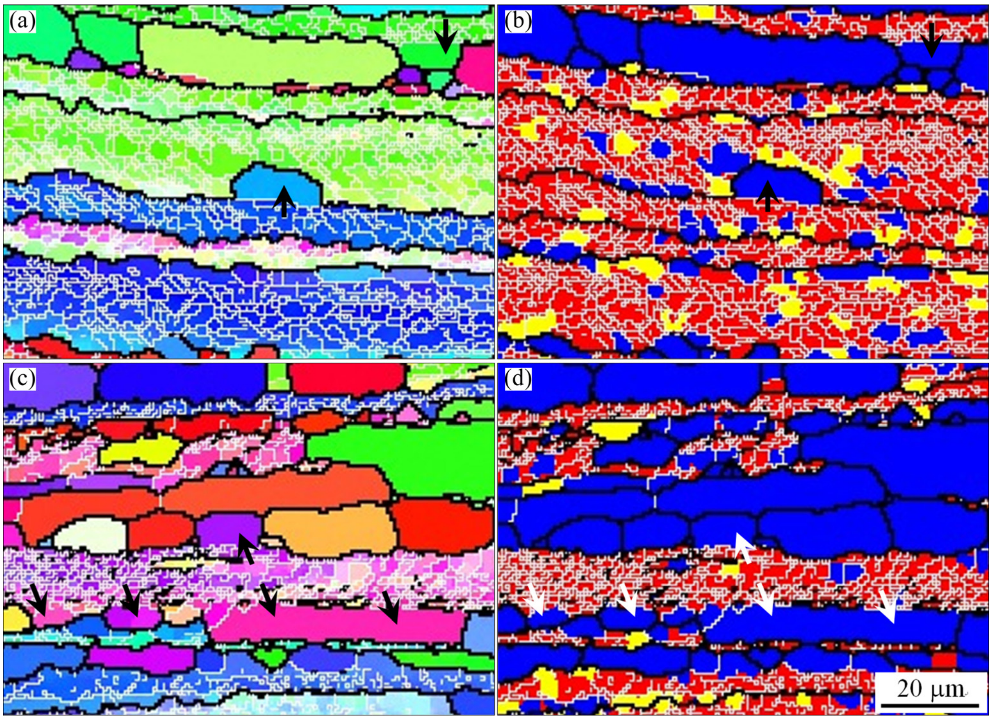

Fig. 13 Magnified local IPF (a, c) and structure distribution (b, d) of sheets with 50% cold reduction after solutionization at 555 °C (a, b) and 575 °C (c, d) (Arrows indicate grain boundary bending model)

In the aged 1445 Al−Li alloy sheet, in addition to dense δ' (Al_3Li) precipitates, there also exist some dispersoids with shell/core structure and a diameter of 20−30 nm (Fig. 14(a)), which were determined as nano-sized $Al_3(Sc,Zr)$ particles in our previous STEM observation [27]. The δ' phases precipitate during the aging process, but the $Al_3(Sc,Zr)$ dispersoids are formed during solidification, thermo-mechanical process and annealing process [29]. The nano-sized $Al_3(Sc,Zr)$ dispersoid is coherent with the Al matrix, of which the orientation relationship is $[110]_{Al_3(Sc,Zr)}//[110]_{Al}$ and $(002)_{Al_3(Sc,Zr)}//(002)_{Al}$ [30]. In addition, the lattice mismatch between $Al_3(Sc,Zr)$ and Al is lower than that between Al_3Sc and Al, and it is decreased with temperature elevation [31]. Furthermore, coherent dispersoids exert a strong Zener drag on dislocations and grain boundaries [32−34]. The non-recrystallization of the solutionized 1445 Al−Li alloy sheet, therefore, is due to the nano-sized $Al_3(Sc,Zr)$ dispersoids.

The role of $Al_3(Sc,Zr)$ particles in impeding recrystallization is evidenced by STEM observation of the 1445 Al−Li alloy sheet with 50% cold reduction after solutionization at 525 °C. The pinning (Zener pinning) of the nano-sized $Al_3(Sc,Zr)$ particles on the subgrain boundaries and dislocations (Fig. 14(b)) is clearly observed. The STEM observation confirms that the nano-sized coherent $Al_3(Sc,Zr)$ particles raise the difficulty of the accumulation of subgrains, stabilize the dislocations and thus hamper the nucleus formation of the recrystallization.

4.2 Effect of cold reduction and solutionization temperature on grain structures

According to the above observations, the recrystallization fraction and the recrystallized grain size are decreased with increasing the cold reduction. However, the recrystallization usually occurs more easily at a higher cold reduction because of higher stored energy, the driving force for the recrystallization. It seems that there exists a discrepancy.

It was reported that during the cold rolling process of Al and Al alloys, as the cold reduction is increased from 50% to 90%, the microstructure evolved from cell-block structure to structure composed of lamellar boundaries (LBs) and inter-connecting cell boundaries [35]. Meanwhile, the fraction of HABs was increased, the main reason of which was that the fraction of deformation-induced HABs increased with the cold reduction [35]. In addition, the number of small volume elements within individual texture components was decreased [36]. Furthermore, the nano-sized $Al_3(Sc,Zr)$ dispersoids pin the grain boundaries and therefore hinder their migration. As a result, no long-range orientation gradient exists along the thickness direction, and the coalescent subgrains may not grow as recrystallized nuclei, because of the absence of HABs around them. These formed sub-structures are still defined as subgrains, and this process is also called as in-situ recrystallization.

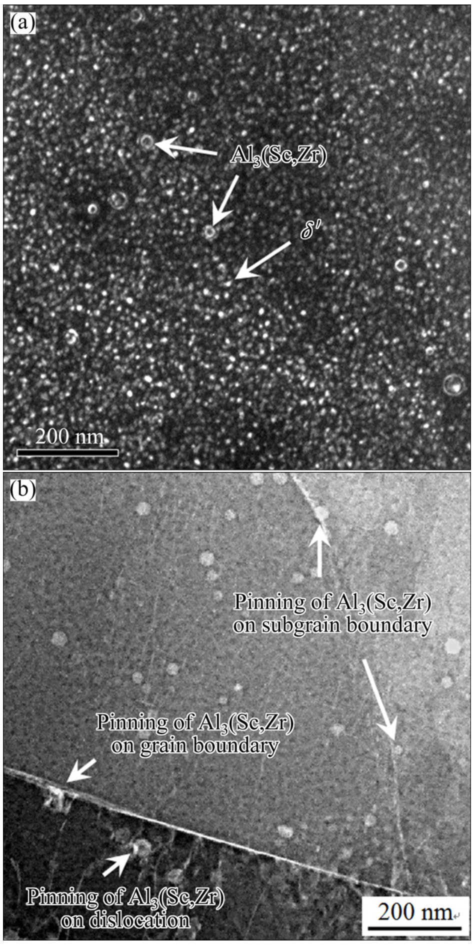

Fig. 14 DF-TEM (a) and BF-STEM (b) images of 1445 Al−Li alloy sheet with 50% cold reduction: (a) δ' precipitates after aging (direction parallel to $\langle 100 \rangle_{\mathrm{Al}}$); (b) Zener pinning of $Al_3(Sc,Zr)$ particles on subgrain boundaries and dislocations

So, although the stored energy is increased with increasing the cold reduction, the fraction of the recrystallization is decreased, which is accompanied with an increase of the fraction of the subgrains and a decrease of the fraction of the deformed structures. In addition, the recrystallization mainly occurs within the band with HABs. Due to the decreased band thickness, the recrystallized grain size is therefore decreased.

Another important phenomenon should be noted. The distribution of the recrystallized grain size shows a wider range at a lower cold reduction (Fig. 5(b)). Furthermore, with increasing the cold reduction, the maximum size of the recrystallized grains is greatly decreased, but the minimum size is just decreased a little. This phenomenon is associated with the band size prior to solutionization. The thickness of band with HABs is much more dispersive at lower cold reduction [36,37], which in turn causes a wider range of the recrystallized grain size. At a higher cold reduction, the fraction of deformation-induced HABs is increased, and the maximum band thickness in the area surrounded by HABs is accordingly decreased, which results in much small recrystallized grain size with narrow distribution range.

The temperature elevation accelerates the volume diffusion, which is necessary for the recrystallization. This also maybe leads to the dissolution of the $Al_3(Sc,Zr)$ dispersoids, because the Sc solubility in Al is increased. However, $Al_3(Sc,Zr)$ possesses a shell/core structure with Zr-rich shell and Sc-rich core. Due to the slower diffusivity of Zr and its existence at the shell, it was reported that the coarsening rate of $Al_3(Sc,Zr)$ dispersoids was much lower than that of Al_3Sc dispersoids [38]. The dissolution rate reasonably displays the same law, due to the same diffusion control. Moreover, the solubility of Zr in Al at 600 °C is between 0.05% and 0.07% (mass fraction) [39], which is much lower than the Zr concentration of the 1445 Al−Li alloy in this case. This impedes the complete dissolution of Zr elements into the matrix. Due to these factors, the $Al_3(Sc,Zr)$ dispersoids are difficult to be completely dissolved into the matrix during the solutionization process at 555 °C, and even at 575 °C for 1 h.

It was reported that the $Al_3(Sc,Zr)$ dispersoids were much stable in cast Al−Mg alloys with Sc and Zr additions at high temperature of 550 °C [40]. However, after hot rolling and cold rolling, dislocations were pinned and connected around the $Al_3(Sc,Zr)$ dispersoids. The $Al_3(Sc,Zr)$ dispersoids were connected by a network of tangled dislocations. It is well known that diffusion of solute atoms along dislocations and boundaries is much easier than that in matrix [40,41]. Due to these two factors, the increased solubility of Zr and Sc elements, and the higher velocity in the deformed alloy at higher temperatures, the $Al_3(Sc,Zr)$ dispersoids can be coarsened when being solutionized at 575 °C. Their number density and volume fraction are lowered, leading to a wider spacing. This phenomenon was also observed in Al−Zn−Mg alloys with small addition of Sc and Zr [25]. As a result, the pinning effect $Al_3(Sc,Zr)$ dispersoids on dislocations, subgrain boundaries and grain boundaries is therefore weakened. The fraction and size of the recrystallized grains are therefore increased. In addition, because the recrystallized grains mainly nucleate and grow inside the band with HABs, the maximum recrystallized grain size is controlled by the band size of the cold-rolled sheet. Accordingly, as the solutionization temperature is elevated to 575 °C, the minimum recrystallized grain size is greatly increased, but there is not much increase in the maximum recrystallized grain size.

4.3 Effect of cold reduction on strength

It is of interest that although the recrystallized grain size is decreased with increasing the cold reduction, the strength of the T8-aged 1445 Al−Li alloy sheet is lowered. The strength heterogeneity shows a similar trend (Fig. 11 and Table 2). This phenomenon can be explained through solutionized grain structure variation caused by different cold reductions.

With increasing the cold reduction, the subgrain fraction is increased. The subgrains and some recrystallized grains possess same features. The subgrains with yellow color in Figs. 1(c), 2(c), 3(c) and 4(c) are formed through subgrain coalescence and growth, while most recrystallized grains are also formed through this mechanism. Their similarity lies in the low dislocation density inside both the subgrains and the recrystallized grains. The difference lies in the HABs at the recrystallized grain boundary, but the LABs at the subgrain boundary. According to the dislocation configuration, these subgrains and recrystallized grains can be considered to have a same structure. Actually, the subgrains are also called as in-situ recrystallized grains. The total fraction of the recrystallized grains (including in-situ recrystallized grains or subgrains) is increased, and that of the deformed structure is decreased with increasing the cold reduction (Fig. 5). In addition, LABs are not effective barriers to the gliding of the mobile dislocations [42]. The decrease of the deformed structure fraction, or the increase of the subgrain fraction contributes to the strength lowering.

Although the fraction of the recrystallized grains is decreased with increasing the cold reduction, the subgrain (in-situ recrystallized grain) fraction is increased, which is accompanied with a number fraction increase of the HABs. As shown in Fig. 6, with increasing the cold reduction, the number fraction of LABs (θ<10°) is decreased, but that of HABs (especially HABs with θ=50−60°) is increased. This effect leads to a lower heterogeneity.

5 Conclusions

(1) Incomplete recrystallization occurs in the solutionized 1445 Al−Li alloy sheet, and the grain structures display as fiber-like grains accompanied with some recrystallized grains. When being solutionized at 575 °C, the alloy sheet still maintains the characteristics of incomplete recrystallization.

(2) With increasing the cold reduction, the fraction of recrystallized grains and their size are lowered. However, it also displays a decrease trend in the fraction of deformed structures, which is accompanied with an increase in the fraction of subgrains. At higher solutionization temperature of 575 °C, the fraction of recrystallized grains and their size are obviously increased.

(3) The main recrystallization model is subgrain coalescence and growth. Nano-sized $Al_3(Sc,Zr)$ dispersoids are observed to pin the grain boundaries, subgrain boundaries and dislocations, which is the cause of the non-recrystallization in the 1445 Al−Li alloy.

(4) The strength and the heterogeneity of the T8-aged 1445 Al−Li alloy sheet are lowered with increasing the cold reduction, which is concomitant with a lower fraction of deformed structures and higher number fraction of the HABs.

References

[1] RIOJA R J, LIU J. The evolution of Al−Li base products for aerospace and space applications [J]. Metallurgical and Materials Transactions A, 2012, 43: 3325−3337.

[2] RIOJA R J, DENZER D K, MOOY D C, VENEMA G. Lighter and stiffer materials for use in space vehicles [C]//WEILAND H, ROLLETT A D, CASSADA W A. Proceedings of 13th International Conference on Aluminum Alloys (ICAA13). Pittsburgh, USA: TMS (The Minerals, Metals & Materials Society), 2012: 593−598.

[3] MAGNUSEN P E, MOOY D C, YOCUM L A, RIOJA R J. Development of high toughness sheet and extruded products for airplane fuselage structures [C]// WEILAND H, ROLLETT A D, CASSADA W A. Proceedings of 13th International Conference on Aluminum Alloys (ICAA13). Pittsburgh, USA: TMS (The Minerals, Metals & Materials Society), 2012: 535−540.

[4] DECREUS B, DESCHAMPS A, de GEUSER F, DONNADIEU P, SIGLI C, WEYLAND M. The influence of Cu/Li ratio on precipitation in Al−Cu−Li−*x* alloys [J]. Acta Materialia, 2013, 61: 2207−2218.

[5] GUMBMANN E, LEFEBVRE W, de GEUSER F, SIGLI C, DESCHAMPS A. The effect of minor solute additions on the precipitation path of an Al−Cu−Li alloy [J]. Acta Materialia, 2106, 115: 104−114.

[6] HUANG B P, ZHENG Z Q. Independent and combined roles of trace Mg and Ag additions in properties precipitation process and precipitation kinetics of Al−Cu−Li−(Mg)−(Ag)−Zr−Ti alloys [J]. Acta Materialia, 1998, 46: 4381−4393.

[7] LEQUEU Ph, SMITH K P, DANIELOU A. Aluminum−copper−lithium alloy 2050 developed for medium to thick plate [J]. Journal of Materials Engineering and Performance, 2010, 19: 841−847.

[8] MURAYAMA M, HONO K. Role of Ag and Mg on precipitation of T1 phase in an Al−Cu−Li−Mg−Ag alloy [J]. Scripta Materialia, 2001, 44: 701−706.

[9] FU B L, QIN G L, MENG X M, JI Y, ZOU Y, LEI Z. Microstructure and mechanical properties of newly developed aluminum−lithium alloy 2A97 welded by fiber laser [J]. Materials Science and Engineering A, 2014, 617: 1−11.

[10] LI J F, XU L, CAI C, CHEN Y L, ZHANG X H, ZHENG Z Q. Mechanical property and intergranular corrosion sensitivity of Zn-free and Zn micro-alloyed Al−2.7Cu−1.7Li−0.3Mg alloys [J]. Metallurgical and Materials Transactions A, 2014, 45: 5736−5748.

[11] TSIVOULAS D, PRANGNELL P B. The effect of Mn and Zr dispersoid-forming additions on recrystallization resistance in Al−Cu−Li AA2198 sheet [J]. Acta Materialia, 2014, 77: 1−16.

[12] TSIVOULAS D, PRANGNELL P B. Comparison of the effect of individual and combined Zr and Mn additions on the fracture behavior of Al−Cu−Li alloy AA2198 rolled sheet [J]. Metallurgical

and Materials Transactions A, 2014, 45: 1338−1351.

[13] YANG X S, CHAI L J, HUANG W J, MA Y L, ZHANG Z H. Texture evolution and microstructural thermal stability of as-extruded AA2099 during hot deformation [J]. Materials Science & Engineering A, 2016, 675: 431−436

[14] KOLOBNEV N I. Aluminum−lithium alloys with scandium [J]. Metal Science and Heat Treatment, 2002, 44: 297−299.

[15] JIANG F, ZHOU J, HUANG H, QU J. Characterisation of microstructure and mechanical properties in Al−Mg alloy with addition of Sc and Zr [J]. Materials Research Innovations, 2014, 18: S4-228−S4-234.

[16] PAN Qing-lin, YIN Zhi-min, Zou Jing-xia, CHEN Xian-ming, ZHANG Chuan-fu. Effects of minor Sc addition on microstructure and tensile property of Al−Mg alloy [J]. Acta Metallurgical Sinica, 2001, 37: 749−753. (in Chinese)

[17] CHEN X M, LUO C P, PAN Q L, YIN Z M. Effects of micro-alloying with Sc and Mn on microstructure and mechanical properties of Al−Mg based alloys [J]. Transactions of Nonferrous Metal Society of China, 2005, 15: 1108−1112.

[18] DENG Y, YIN Z M, ZHAO K, DUAN J Q, HE Z B. Effects of Sc and Zr microalloying additions on the microstructure and mechanical properties of new Al−Zn−Mg alloys [J]. Journal of Alloys and Compounds, 2012, 530: 71−80.

[19] LI B, PAN Q L, X HUANG, YIN Z M. Microstructures and properties of Al−Zn−Mg−Mn alloy with trace amounts of Sc and Zr [J]. Materials Science and Engineering A, 2014, 616: 219−228.

[20] LIU J, YAO P, ZHAO N Q, SHI C S, LI H J, LI X, SI D S, YANG S. Effect of minor Sc and Zr on recrystallization behavior and mechanical properties of novel Al−Zn−Mg−Cu alloys [J]. Journal of Alloys and Compounds, 2016, 657: 717−725.

[21] MA J, YAN D S, RONG L J, LI Y Y. Effect of Sc dddition on microstructure and mechanical properties of 1460 alloy [J]. Progress in Natural Science—Materials International, 2014, 24: 13−18.

[22] ZHANG Hai-feng, ZHENG Zi-qiao, LIN Yi, XUE Xi-li, LUO Xain-fu, ZHONG Jing. Effects of small addition of Sc on microstructure and properties of 2099 Al−Li alloy [J]. Journal of Central South University (Science and Technology), 2014, 45: 1420−1427. (in Chinese)

[23] LIU Dan-yang, WANG Jie-xia, LI Jin-feng. The microstructures evolution and mechanical properties disparity in 2070 Al−Li alloy with minor Sc addition [J]. Transactions of Nonferrous Metals Society of China, 2018, 28: 2151−2161.

[24] MA Y L, LI J F. Variation of aging precipitates and strength of Al−Cu−Li alloys caused by small addition of rare earth elements [J]. Journal of Materials Engineering and Performance, 2017, 26: 4329−4339.

[25] DENG Y, XU G F, YIN Z M, LEI X F, HUANG J W. Effects of Sc and Zr microalloying additions on the recrystallization texture and mechanism of Al−Zn−Mg alloys [J]. Journal of Alloys and Compounds, 2013, 580: 412−426.

[26] OVSYANNIKOV B V, POPOV V I. Development of a new aluminium−lithium alloy of Al−Cu−Mg−Li (Ag, Sc) system intended for manufacturing sheets, thin-walled sections and forgings [C]//KUMAI S, UMEZAWA O, TAKAYAMA Y, TSUCHIDA T, SATO T. Proceedings of the 12th International Conference on Aluminium Alloys (ICAA12). Yokoha, Japan: The Japan Institute of Light Metals, 2010: 441−446.

[27] PENG Z W, LI J F, SANG F J, CHEN Y L, ZHANG X H, ZHENG Z Q, PAN Q L. Structures and tensile properties of Sc-containing 1445 Al−Li alloy sheet [J]. Journal of Alloys and Compounds, 2018, 747: 471−483.

[28] GAO C, LUAN Y, YU J C, MA Y. Effect of thermo-mechanical treatment process on microstructure and mechanical properties of 2A97 Al−Li alloy [J]. Transactions of Nonferrous Metal Society of China, 2014, 24: 2196−2202.

[29] HUANG H F, JIANG F, ZHOU J, WEI L L, QU J P, LIU L L. Effects of $Al_3(Sc,Zr)$ and shear band formation on the tensile properties and fracture behavior of Al−Mg−Sc−Zr alloy [J]. Journal of Materials Engineering and Performance, 2015, 24: 4244−4252.

[30] WANG Y, PAN Q L, SONG Y F, LI C, LI Z F, CHEN Q, YIN Z M. Recrystallization of Al−5.8Mg−Mn−Sc−Zr alloy [J]. Transactions of Nonferrous Metal Society of China, 2013, 23: 3235−3241.

[31] HARADA Y, DUNAND D C. Thermal expansion of Al_3Sc and $Al_3(Sc_{0.75}X_{0.25})$ [J]. Scripta Materialia, 2003, 48: 219−222.

[32] STIDIKOV O, SAKAI T, AVTOKRATOVA E, KAIBYSHEV R, TSUZAKI K, WATANABE Y. Microstructure behavior of Al−Mg−Sc alloy processed by ECAP at elevated temperature [J]. Acta Materialia, 2008, 56: 821−834.

[33] BURANOVA Y, KULITSKIY V, PETERLECHNER M, MOGUCHEVA A, KAIBYSHEV R, DIVINSKI S V, WILDE G. $Al_3(Sc,Zr)$-based precipitates in Al−Mg alloy: Effect of severe deformation [J]. Acta Materialia, 2017, 124: 210−224.

[34] WANG N, WEN Y, CHEN L Q. Chen. Pinning force of grain boundary migration by a coherent particle [J]. Philosophical Magazine Letters, 2014, 94: 794−802.

[35] YAO Zong-yong, LIU Qing, GODFREY A, LIU Wei. Microstructure and texture evolutioins of AA1050 aluminum alloy cold rolled to high strains [J]. Acta Metallurgica Sinica, 2009, 45: 647−651. (in Chinese)

[36] YAO Z Y, ZHANG Z Q, GODFREY A, LIU W, LIU Q. Microstructure and texture evolution of particle-containing AA3104 alloy cold rolled to large strains [J]. Materials Science and Technology, 2010, 26: 539−546.

[37] YAO Z Y, HUANG G J, GODFREY A, LIU W, LIU Q. Dislocation boundary structure from low to medium strain of cold rolling AA3104 Al alloy [J]. Metallurgical and Materials Transactions A, 2009, 40: 1487−1497.

[38] FORBORD B, LEFEBVRE W, DANOIX F, HALLEM H, MARTHINSEN K. Three dimensional atom probe investigation on the formation of $Al_3(Sc,Zr)$-dispersoids in aluminium alloys [J]. Scripta Materialia, 2004, 51: 333−337.

[39] ROKHLIN L L, BOCHVAR N R, BOSELLI J, DOBATKINA T V. Investigation of the Al-rich part of the Al−Zr−Hf phase diagram for solid state [J]. Journal of Phase Equilibria and Diffusion, 2010, 31: 504−508.

[40] DU Gang, YAN De-sheng, RONG Li-jian. Influence of intermediate annealing temperatures on mechanical properties of repeatedly cold-rolled Al−Mg−Sc−Zr alloy [J]. Acta Metallurgica Sinica, 2008, 44: 1209−1212. (in Chinese)

[41] DU G, DENG J W, YAN D S, ZHAO M J, RONG L J. Coarsening behavior of $Al_3(Sc,Zr)$ precipitates and its influence on recrystallization temperature of Al−Mg−Sc−Zr alloy [J]. Journal of Materials Science and Technology, 2009, 25: 749−752.

[42] HU T, MA K, TOPPING T D, SALLER B, YOUSEFIANI A, SCHOENUNG J M, LAVERNIA E J. Improving the tensile ductility and uniform elongation of high-strength ultrafine-grained Al alloys by lowering the grain boundary misorientation angle [J]. Scripta Materialia, 2014, 78−79: 25−28.

冷轧变形量对铝锂合金薄板晶粒组织及力学性能的影响

马云龙[1,2]，李劲风[1,3]，桑冯建[1]，李红英[1]，郑子樵[1]，黄 诚[4]

1. 中南大学 材料科学与工程学院，长沙 410083；
2. 北京宇航系统工程研究所，北京 100076；
3. 中南大学 有色金属材料科学与工程教育部重点实验室，长沙 410083；
4. 中南大学 轻合金研究院，长沙 410083

摘 要：采用电子背散射衍射(EBSD)研究冷轧变形量(50%~90%)对 1445 铝锂合金薄板固溶态(固溶温度 525~575 °C) 晶粒组织的影响。薄板固溶时再结晶模式为亚晶合并与生长，但固溶温度提高至 575 °C 时薄板仍然未发生完全再结晶。未再结晶是由于添加微量 Sc 元素形成纳米尺寸 $Al_3(Sc, Zr)$粒子，钉扎晶界、亚晶界及位错所致。525 °C 固溶时，随冷轧变形量增加，薄板再结晶分数及再结晶晶粒尺寸减小，但亚晶分数增加，相应变形组织分数减少；同时，大角度晶界分数增加；这两个原因导致薄板 T8 时效后强度及各向异性随冷轧变形量增加而降低。固溶温度提高至 575 °C 时，再结晶分数及再结晶晶粒尺寸增加。

关键词：铝锂合金；晶粒组织；再结晶；强度；冷轧变形量

(Edited by Bing YANG)